ESRF	**Experiment title:** *Non-destructive compositional and structural investigations of inclusions in sub-lithospheric diamonds*	**Experiment number**: CH 1780
Beamline:	**Date of experiment**: (long term) from: July 2004 to: December 2005	**Date of report**: 10 January 2006
Shifts: 63 (until now)	**Local contact(s)**: Dr Rémi Tucoulou Dr Sylvain Bohic Dr Gema Martinez-Criado	*Received at ESRF:*

Names and affiliations of applicants (* indicates experimentalists):

Proposer: *(to whom correspondence will be addressed*) ***Prof. K. Janssens, *Dr. B. Vekemans**

Address: Micro Trace Analysis Centre (MiTAC), Department of Chemistry, University of Antwerp (UA), Universiteitsplein 1, B-2610 Antwerp

***Prof. L. Vincze,**

Address: Dept. Analytical Chemistry, Ghent University, Krijgslaan 281, B-9000 Gent

***Dr. F. Brenker**

Address: Inst. Mineralogy, Univ. of Frankfurt, Senckenberganlage 28, D-60054 Frankfurt

0. Table of content

1. Long term project, general aspects of experimental sessions
2. Experimental sessions
    2.a. Experimental session 1 (28 January – 5 February 2005, 21 shifts)
    2.b. Experimental session 2 (16-24 June 2005, 21 shifts)
    2.c. Experimental session 3 (11-18 November 2005, 21 shifts)
3. Planned experimental sessions
4. Publications
5. Conferences and Meetings

1. Long term project, general aspects of experimental sessions

The period of the long term project extends from July 2004 to July 2006. Until now 63 shifts were used during three experimental sessions described below.

Inclusions of diamonds from two different origins, Juina and Kankan, were measured using the confocal XRF imaging technique (single volume element measurement, line scan, slice or full 3D) and scanning XRD (single point or 2D). The investigation of the series of inclusions within different diamonds was complemented with micro-Raman studies (not mentioned in this report) and with an experimental session at HASYLAB beamline L for REEs determination (see indication "*" in the sample list of experimental session 1).

Wout De Nolf, a PhD student of Prof. K. Janssens, started the development of a program to automate the evaluation of single and series of diffraction images. Anja Szymanski joined the group of Dr. F. Brenker with the specific task to interprete the XRD images.

Although the evaluation and interpretation of the XRF/XRD data of many of the data sets collected during the experimental sessions is still in progress, a number of extremely interesting and novel findings already could be observed.

2. Experimental sessions

2.a. Experimental session 1 (28 January – 5 February 2005, 21 shifts)

Participants : R. Tucoulou, K. Janssens, L. Vincze, F. Brenker, B. Vekemans
Topic : identification of inclusions in diamonds
Experimental set-up : confocal XRF imaging base of polycapillary lenses, complementary micro-XRD where necessary; 28 keV, beamsize typically 2 μm (V) × 10 μm (H), polycapillary acceptance 22 μm (Au-L).
Overview :

RS68-diamond			
	RS68-C	multiphase + walstromite	**3D-XRF + 2D diffractionmap** *
	RS68-E	walstromite	P (XRF + XRD) *
	RS68-G	calcite	P (XRF + XRD)
	RS68-F	calcite ?	P (no XRF response, XRD)
RS35-diamond			
	RS35-B	calcite	**3D-XRF**, P (XRF + XRD) *
	RS35-A2	walstromite	line-scans
	RS35-C	calcite ?	P (XRF)
	RS35-A	walstromite	P (XRF, XRD)
RS37 diamond			
	RS37-A	walstromite	**3D-XRF + 2D diffractionmap** *
	RS37-small	?	P (XRF, XRD)
	RS37-crack	Fe-rich	P (XRF)
RS63 diamond			
	RS63-B	calcite polished to the surface	slice through inclusion (XRF)
RS53 diamond			
	RS53-C	Al2O3 or (Mg)O ?	no XRF, XRD line scans
	RS53-B	not well defined by Raman	no XRD signal
RS56 diamond			
	RS56-B	?	no XRF signal
	RS56 Fe-Ni	magnetite from Raman	slice through inclusion (XRF)
			P (XRF, XRD)
			XRD map on subarea 5
	RS56-E	magnetite	P (XRF, XRD)
	RS56-C2	strong Fe signal	P (XRF, XRD)
	RS56-F	?	P (XRF, XRD)
	RS56-G	low Z material	no XRF signal
RS69 diamond (RS69C: trapped multiphase melts or fluids)			
	RS69-C1	magnetite	P (XRF)
	RS69-C2	?	line scans (XRF, XRD)
	RS69-C3-4	-	no XRF signal
	RS69-C5	?	slice through inclusion (XRF)
			P (XRF)
	RS69-C9	black inclusion	P (XRF)
	RS69-C10	?	**3D-XRF**
	RS69-C13	Zn-rich + Ca	P (XRF)

RS69-C14	?	P (XRF)
RS69-C[15-18]	fluid inclusions ?	P (XRF)

"P" indicates single point measurements
"*" indicates additional measurements for REE determination (capillary optics, 30 micron polychromatic X-ray beam) performed in June 2004 at HASYLAB beamline L.

As an example, below the distributions of a number of transition metals in an area populated by a number of fairly small inclusions RS69-C[15-18] are shown. Although positioned close together, very large differences in the composition of the inclusions are noticeable, as can be seen in the two sum spectra that are shown. Both inclusions contain Fe as a major compoment, but one of them is associated with Cr and Ni while in the other Mn is present at a concentration level ca. 30-50 times lower than Fe.

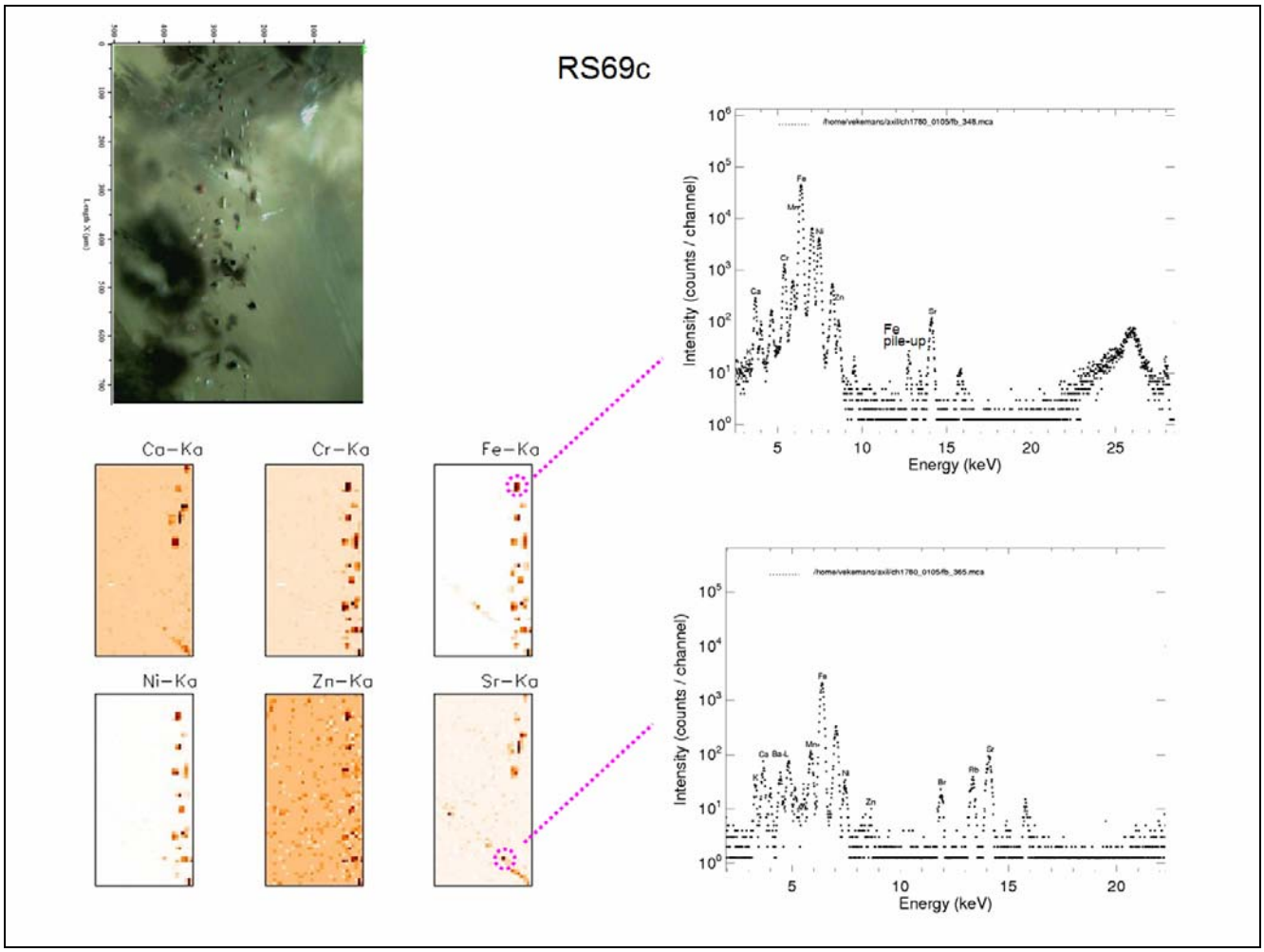

Fig. 1. (left) Optical photograph, elemental distributions and (right) a few representative XRF spectra derived from one plane of analysis position through a series of small inclusions close to inclusion RS69c.

However, as can be noticed in the XRF maps shown above, the beam size employed is not really small enough to allow the analysis of details within the small (5-10 μm diameter) inclusions.

In the XRF maps shown below, collected through the middle of inclusion RS68c, a complex intergrowth of several Ca-rich phases is visible; a CaTi-phase, a Zr-rich phase and a Y-rich phase are discernable. In the Ti-rich region, the XRD data show a prominent peak at d = 3.8 Å, suggesting that we may be dealing here with an CaTi-perovskite structure. Thus, this inclusion is likely to consist of walstromite-structured $CaSiO_3$ and $CaTiO_3$. Such a phase assemblage can be interpreted as a former $CaSi_{1-x}Ti_xO_3$-perovskite solid solution, requiring a minimum pressure of ca 9.5GPa to form.

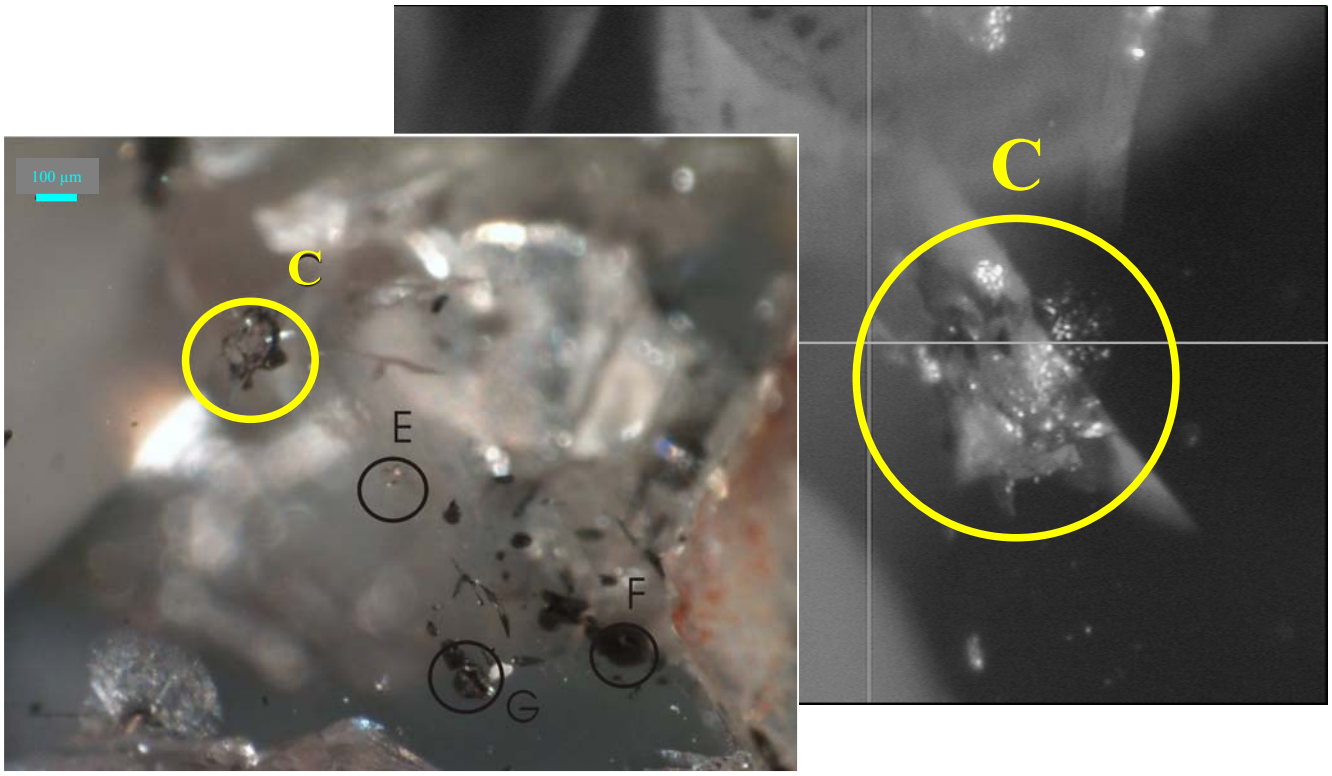

Fig. 2. Optical photographs of inclusions RS68c,e,f and g.

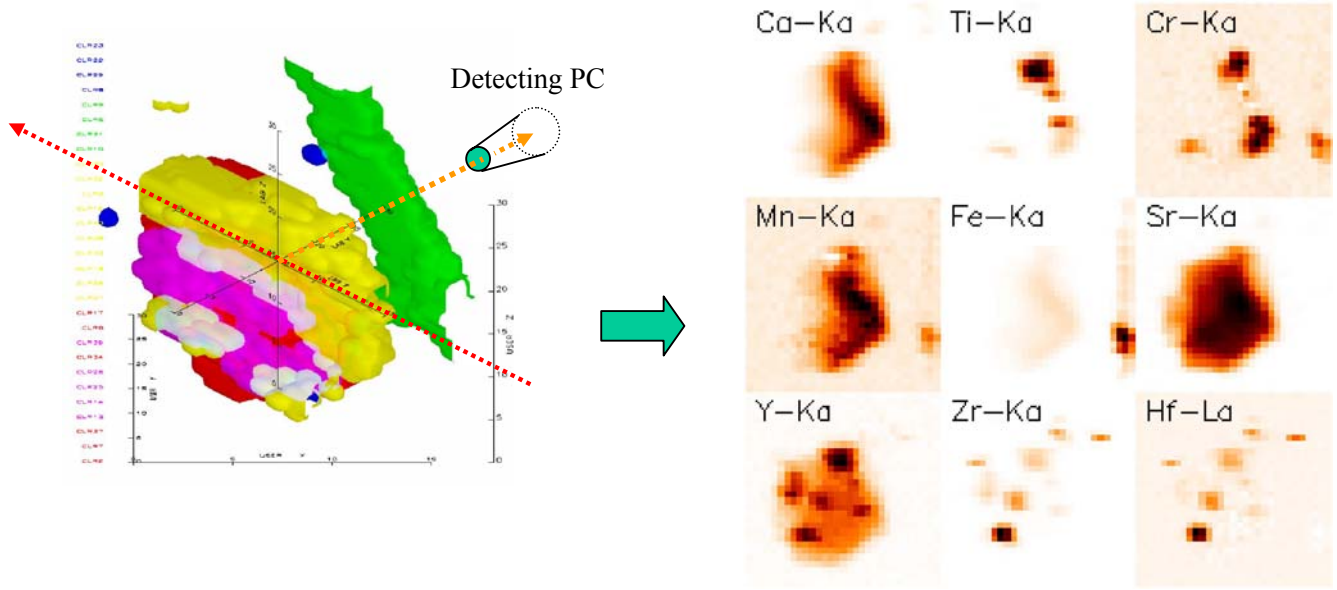

Fig. 3 (left) 3D reconstruction of the distribution of various phases inside inclusion RS68c; (right) projected 2D distributions aliong dashed arrow shown in left panel.

2.b. Experimental session 2 (16-24 June 2005, 21 shifts)

Participants : Sylvain Bohic, Gema Martinez-Criado, K. Janssens, L. Vincze, F. Brenker, Anja Szymanski, B. Vekemans

Topic : identification of inclusions in diamonds

Experimental set-up : confocal XRF imaging base of polycapillary lenses, complementary micro-XRD where necessary; 28 keV, beamsize typically 2 µm (V) × 10 µm (H), polycapillary acceptance 22 µm (Au-L).

Overview :

"P" indicates single point measurements

KK106 diamond		
KK106-f	?	line scan (XRF, XRD)
KK106-g	red inclusion	line scan (XRF, XRD)
KK106-h	?	no XRF signal, XRD line scan
KK106-c	garnet	no XRF signal, XRD line scan
KK106-d	single crystal ?	slice through inclusion (XRF)
RS36 diamond		
RS36-a	?	slice through inclusion (XRF)
RS36-b	?	no XRF signal, P (XRD)
RS43 diamond		
RS43-a	Fe-rich phase	P (XRF, XRD) Slice through inclusion (XRF) + XRD map
RS43-B	not possible to find	
RS43-D	no XRF signal	
RS66 diamond		
RS66-D	Fe-rich	P (XRF, XRD)
RS66-E	Fe-rich	P (XRF, no XRD)
RS66-A	40 micron	slice through inclusion (XRF) + XRD line scan
RS66-A2	?	P (XRF)
RS65 diamond		
RS65-B	?	slice through inclusion (XRF) + XRD map
RS58 diamond		
RS58-a	?	no XRF/XRD signals
KK200 diamond		
KK200-3	multiphase	**3D-XRF** + XRD map
KK200-8	Pb	XRD line scan
KK200-4	REEs !	**3D-XRF**

KK200 is a large and colourless diamond containing several inclusions of size 10-100 μm or larger. A darker halo surrounds a number of the inclusions, likely to be caused by a volume increase of the inclusion, causing radial fractures and a partial transformation of the adjacent diamond into graphite. The cracks appear under the optical microscope as black, wing-like appendices of the quasi-spherical inclusions.

As an example, a series of images [12 slices, each 15 μm apart, each consisting of 26 × 51 pixels (3x5 μm^2 in size)] of the Th and the La distribution in inclusion KK200-4 are shown in Fig. 4.

Inside the inclusion proper, an outer shell, enriched in REE and related elements, and also enriched in Fe, Sr, Zr, Pb and Th can be distinguished from the inner core, which does not yield any measureable XRF or XRD signals, possibly indicating the presence of amorphous SiO_2 or of CO_2 in fluid form at the core.

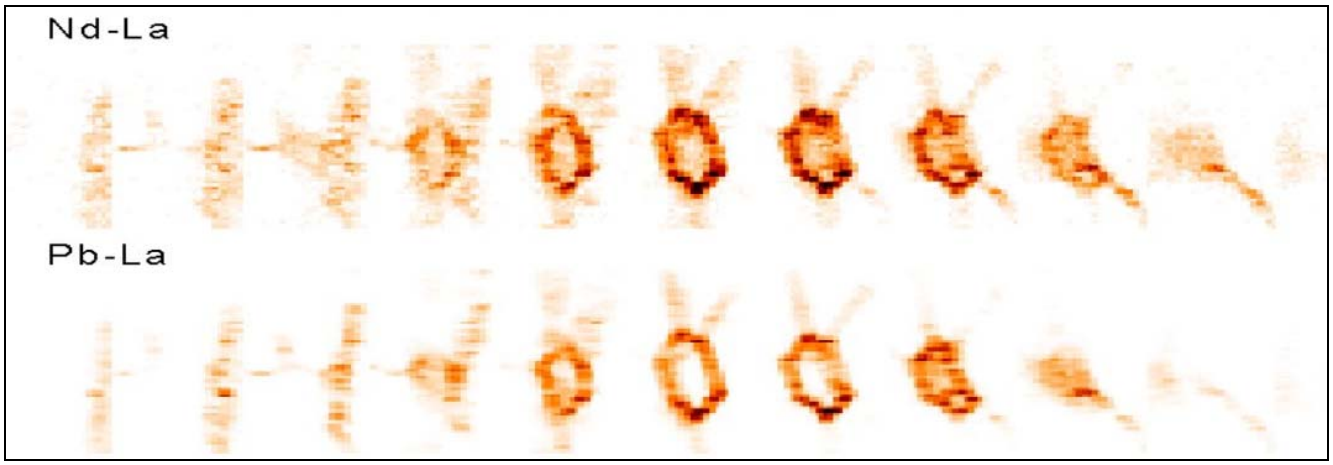

Fig. 4. Elemental distributions of Nd and Pb in a series of planes intersecting inclusion Kankan200#4.

2.c. Experimental session 3 (10-18 November 2005, 21 shifts)

Participants : G. Martinez-Criado, K. Janssens, L. Vincze, A. Szymanski, B. Vekemans, V. Naszmov
Topic : evaluation of SU-8 CRL lens - identification of inclusions in diamonds
Experimental set-up : confocal XRF imaging base of polycapillary lenses, complementary micro-XRD where necessary; 28 keV, beamsize typically 1 μm (V) × 1 μm (H), polycapillary acceptance 22 μm (Au-L).

Overview

The first 1½ days of this experiment were devoted to the alignment and characterization of a newly developed SU-8 CRL lens by ANKA GmbH. To this effect, Dr. V. Nazmov of ANKA GmbH joined us at the start of the experiment (from 10/11/05 to 13/11/05). By gradual adjustments of the number of horizontal and vertical CRL lenses in the series designed for 28 keV, an X-ray beam with quasi circular cross-section could be produced, with an effective diameter of 1 μm and comparable intensity as obtained with the 'standard' Al-CRL lenses available at ID18F. The smallest beam size measured was 0.6 x 0.4 μm^2. A thin gold test-structure, provided by V. Nazmov was used to measure the beam size. Thus, considerably higher resolution 2D images could be recorded than in the previous experimental sessions, where the beam size was typically 2 x 10 μm^2. A high-intensity, high-energy beam with cross-section of ca 1 μm diameter is very convenient for examining inclusions in diamonds down to ca 5 μm diameter.

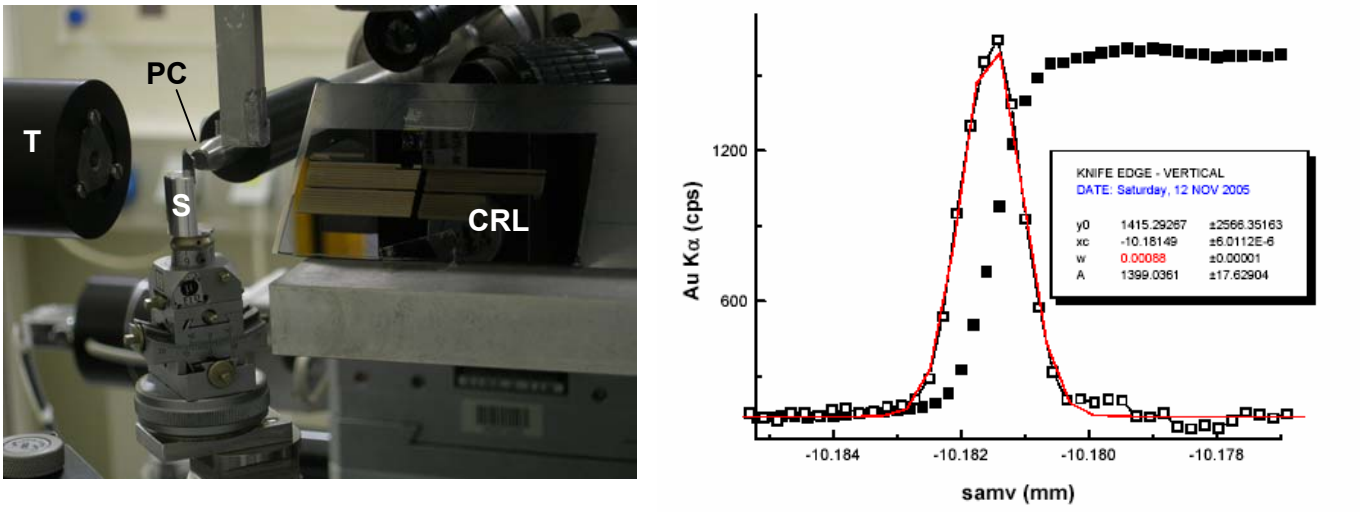

Fig. 5. (left) Photograph of the arrangement of CRL-lens, PC (polycapillary) lens, sample (S) and X-ray transmission camera (T); (right) vertical profile obtained by scanning a thin Au-edge through the primary beam.

Because of the short focal distance of the newly characterized CRL lens (ca 2 cm), a fairly compact geometry around the sample needed to be employed, as shown in the photograph below. The geometrry and the efficiency of the CRL lens were regularly monitored during our experiment and that following us (18-11-05 – 22-11-05;no decrease in performance or other signs of radiation-induced degradation was noticed during this 10 day period.
On 22-11-05, a vertical beamsize of ca 1.5 um was recorded, probably due to slight misaligment of the lens relative to the cross-collimator slits used in front and due to the use of a fairly large opening of these slits. Before the detector, a short (3 cm long) polycapillary lens was used to select the depth in the sample from which the fluorescent radiation can reach the detector. Due to the shorter overall distance the fluorescent photons need to travel through the glass channels of the lens, a 5x larger fluorescent yield for the transition elements was realised. This factor of 5 compensates the losses in primary flux associated with the use of the more strongly focussing CRL lens in combination with the cross-slits.

The following diamond inclusions were measured for the first time or remeasured with higher resolution:

(a) in conventional XRF mode, inclusion Kankan200#4 (RS-35) was scanned again, in order to obtain the total projected distribtion of the REE and other elements at higher resolution. In the previous experiment, this inclusion was already investigated with confocal µ-XRF, but by means of a larger primary beam. The graphite 'wings' are clearly visible in the resulting elemental maps (100x100 points) since they are enriched in the elements that are enriched in the rim of the inclusion proper.

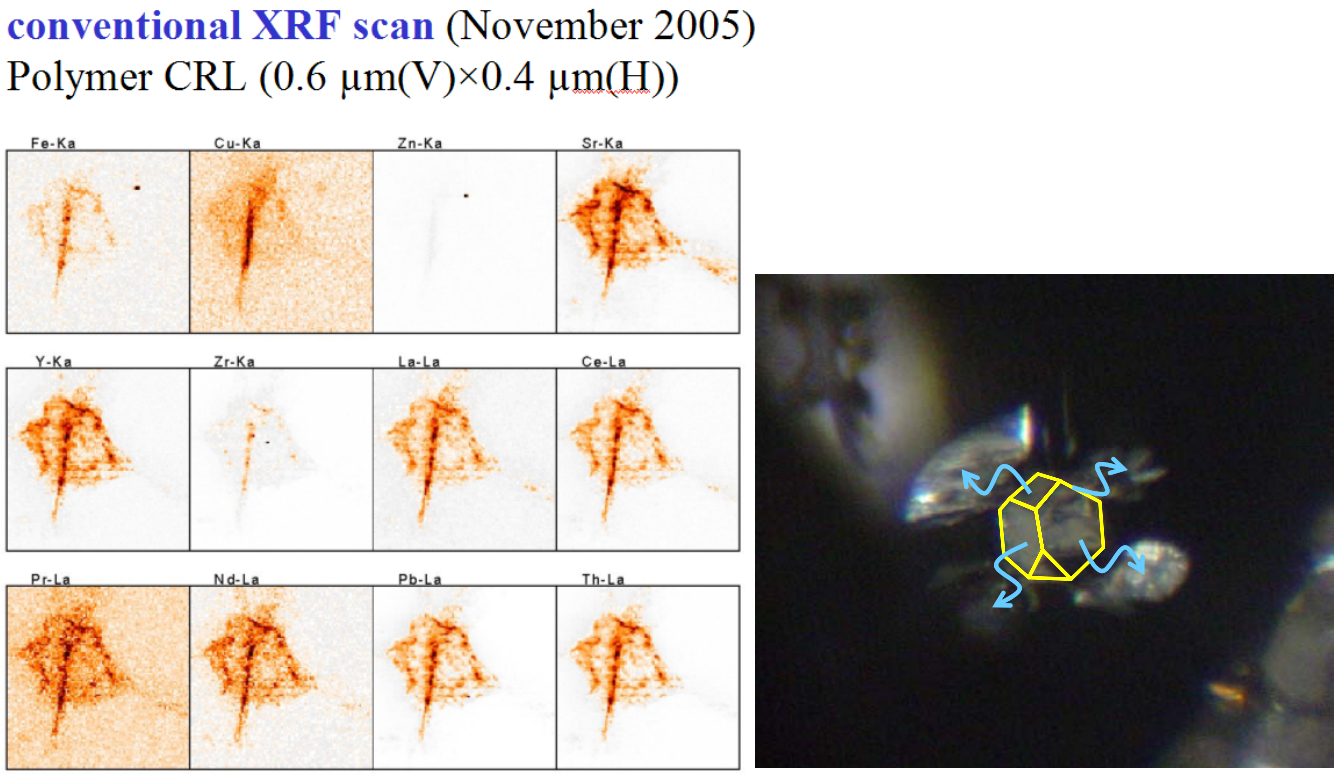

Fig. 6. Projected elemental distributions of different elements through inclusion Kankan200#4 (imaged area: 150 x 150 μm^2).

(b) in confocal XRF mode, the following inclusions were measured by combined XRD and confocal XRF:

RS59 diamond

RS59-a	dolomite, magnesian calcite	XRF + XRD
RS59-b	coexisting carbonates	XRF + XRD
RS59-c	calcite + dolomite, chromite (?)	XRF + XRD
RS59-e	dolomite, chromite	XRF + XRD

RS02 diamond		
RS02-b1	pyrite – all peaks present	XRF + XRD
RS02-c	pyrite - all peaks present	XRF + XRD
RS03 diamond		
RS03-a	olivine + Mg-fayalite ?, forsterite, ringwoodite ?	XRF + XRD
RS03-b	enstatite (?), graphite, larnite, chromite (?), magnesite (?)	XRF + XRD
RS03-d	(?)	XRF + XRD
RS04 diamond		
RS04-a	ferro-periclase	XRF + XRD
RS04-b	(?)	XRF + XRD
RS04-d	(?)	XRF + XRD
RS14 diamond		
RS14-a	pyrrhotite	XRF + XRD
RS14-b	pyrrhotite	XRF + XRD
RS25 diamond		
RS25-a	majoritic garnet + ortho-pyroxene	XRF + XRD
RS25-b	garnet + ? – very clear XRD rings + spots, Fe hot spot	XRF + XRD
RS27 diamond		
RS27-a	ferro-periclase	XRF + XRD
RS42 diamond		
RS42-a	pyrrhotite with attached phases	XRF + XRD
Kankan200-#4	REE, several phases	high-res. XRF

As an example, Fig. 6 shows part of a diffractogram recorded from inclusion RS59-e, where powder rings of a mixture of chromite (e.g., at d = 1.47, 1.60, 2.5 Å) and dolomite (e.g., at *d* = 1.8, 2.0, 2.2, 2.7 Å) are visible.

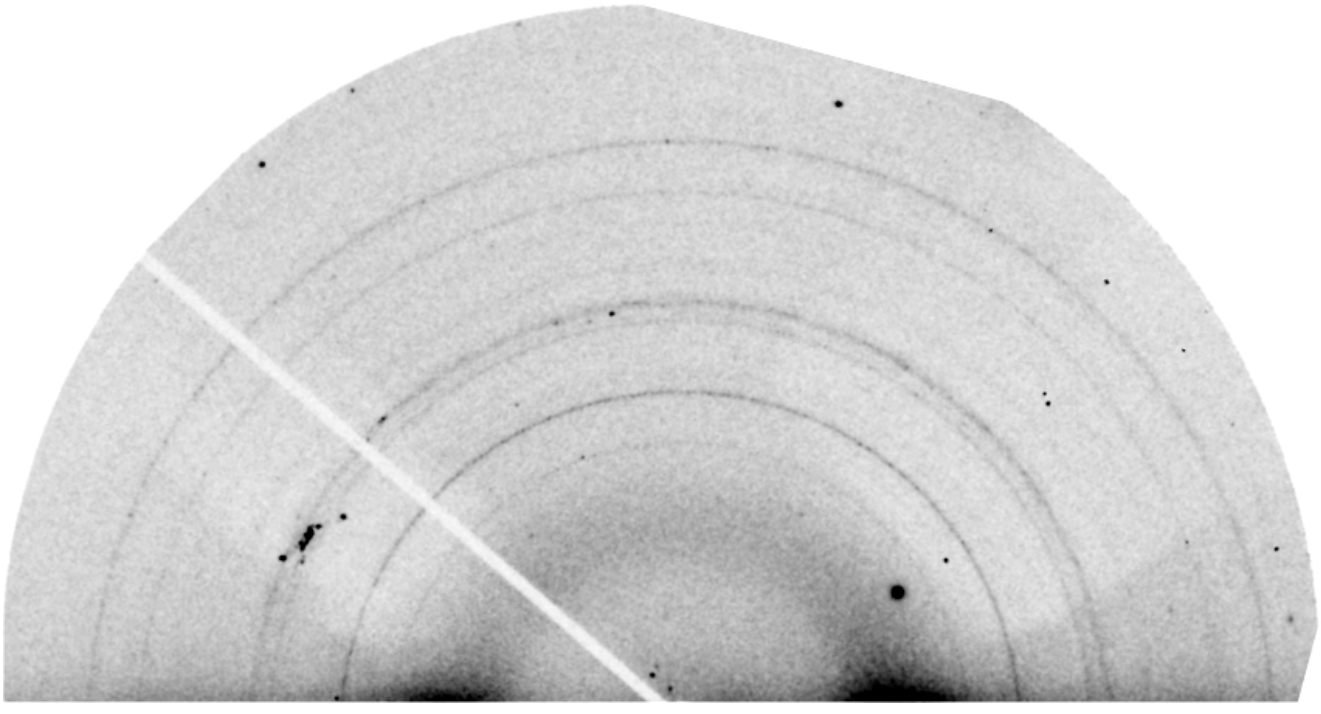

As an example of XRF data, the high resolution maps (100x100 pixels of 1 x 1 μm^2) of the some REE in the central plane through the Kankan200-#4 inclusion are shown below.

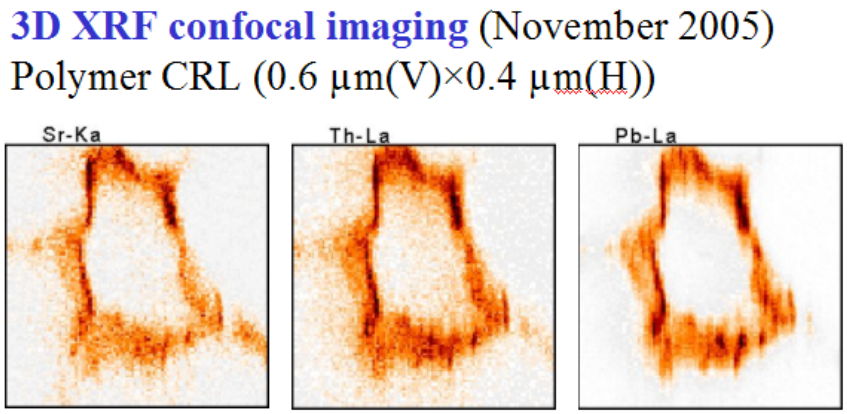

Fig. 7. Sr, Th and Pb-distributions in the central plane of inclusion Kankan200#3 (imaged area: 100 x 100 μm^2).

The co-localization of the elements Fe, Sr, Th and Pb is clearly visible in these maps. In comparison to the conventional XRF maps shown above, the clearly the distribution of elements within the outer shell of the inclusion is shown. Also the existence of small rectangular Pb- and Th-rich crystals, a few micrometers in size near the outer surface of the inclusion are visible.

3. Planned experimental sessions

More high resolution local X-ray fluorescence tomography are planned to study reaction volumes within composite diamond inclusions. These high-resolution studies will require the installation of the new generation of polymer CRLs with sub-micron capabilities. These lenses were manufactured by the Forschungszentrum Karlsruhe and acquired by the MiTAC group.

4. Publications

- L. Vincze, B. Vekemans, F. E. Brenker, G. Falkenberg, K. Rickers, A. Somogyi, M Kersten, and F. Adams; "Three-dimensional trace element analysis by confocal X-ray microfluorescence imaging"; Analytical Chemistry 76 (22), 6786-6791, 2004.
  Abstract. A three-dimensional (3D) variant of scanning micro X-ray fluorescence (XRF) is described and evaluated at the ID18F instrument of the European Synchrotron Radiation Facility (ESRF). The method is based on confocal excitation/detection using a polycapillary half-lens in front of the energy dispersive detector. The experimental arrangement represents a significant generalization of regular twodimensional (2D) scanning micro-XRF and employs a detector half-lens whose focus coincides with that of the focused incoming beam. The detection volume defined by the intersection of the exciting beam and the energy dependent acceptance of the polycapillary optics is 100-350 μm^3. Minimum detection limits are sub-ppm and sensitivities are comparable with regular scanning XRF. Next to the reduction of in-sample single/multiple scattering, the set-up provides the possibility of sample depthscans with an energy dependent resolution of 10-35 µm in the energy range of 3-23 keV, and the possibility of performing 3D-XRF analysis by simple XYZ linear scanning. This provides a suitable alternative to X-ray fluorescence tomography. The method is illustrated with results of the analysis of solid inclusions in diamond and fluid inclusions in quartz.
- B. Vekemans, L. Vincze, F. E. Brenker, F. and Adams; "Processing of three-dimensional microscopic X-ray fluorescence data"; J. Anal. At. Spectrom., 19 (10), 1302 – 1308, 2004.
  Abstract. A novel polycapillary based confocal X-ray fluorescence (XRF) technique was applied for the first time at the ID18F beamline of the ESRF to obtain directly 3-dimensional (3D) compositional information of an inclusion inside a natural diamond sample (KK200). Preliminary analysis of the results

on the basis of the trace elements Sr, Y/Zr, and Th suggest three phases, two of which were identified by earlier micro-Raman spectroscopy as larnite (β-Ca_2SiO_4) and $CaSiO_3$-walstromite, two minerals with significantly different Ca content. In order to support this multiphase model for the investigated inclusion the data set was analysed combining the conventional multivariate method of PCA and K-means clustering procedure after application of instrument specific routines such as spectral evaluation and normalization. Through the knowledge of the full spatial 3D structure of the different phases, it was possible to correct for absorption of the fluorescent radiation in the different phases of the inclusion and the surrounding diamond.

- F. E. Brenker, L. Vincze, B. Vekemans, L. Nasdala, T. Stachel, M. Kersten, A. Somogyi, C. Vollmer, F. Adams, W. Joswig & J. W. Harris; "Evidence for a Ca-rich lithology in the Earth's deep upper mantle"; Earth and Planetary Science Letters, 2005, in press.
  Abstract. Earth's deep convecting upper mantle is believed to represent a rather homogenous geochemical reservoir of spinel or garnet lherzolite with primitive major element and moderately depleted trace element composition. Only where subduction occurs is this homogeneity disrupted by a suite of rocks ranging from eclogites/garnet pyroxenites (former oceanic crust) to residual harzburgites. In addition to these well documented peridotitic and metabasaltic rocks we have now discovered the presence of a chemically distinct reservoir in the deep upper mantle. In situ structural analyses (micro X-ray diffraction and micro Raman spectroscopy) and three-dimensional trace element mapping (confocal micro X-ray fluorescence imaging) of polyphase inclusions in a diamond from Guinea that formed at about 300-360 km depth reveal the existence of a deep Ca-rich source, in the absence of several common mantle minerals, like olivine, garnet and Ca-poor pyroxene. This reservoir may represent metasomatized oceanic lithosphere (rodingites, ophicarbonates) or metamorphosed carbonaceous sediments.
- R. Terzano, M. Spagnuolo, L. Medici, B. Vekemans, L. Vincze, K.Janssens, P. Ruggiero; "Copper stabilization by zeolite synthesis in polluted soils treated with coal fly ash"; Environmental Science and Technology, 39(16), 6280-6287, 2005.
  Abstract. This study deals with the process of zeolite formation in an agricultural soil artificially polluted by high amounts of Cu (15 mg of Cu/g of soil dry weight) and treated with fused coal fly ash at 30 and 60 °C and how this process affects the mobility and availability of the metal. As a consequence of the treatment, the amount of dissolved Cu, and thus its mobility, was strongly reduced, and the percentage of the metal stabilized in the solid phase increased over time, reaching values of 30% at 30 °C and 40% at 60 °C. The physicochemical phenomena responsible for Cu stabilization in the solid phase have been evaluated by EDTA sequential extractions and synchrotron radiation based X-ray microanalytical techniques. These techniques were used for the visualization of the spatial distribution and the speciation of Cu in and/or on the neo-formed zeolite particles. In particular, micro XRF (X-ray fluorescence) tomography showed direct evidence that Cu can be entrapped as clusters inside the porous zeolitic structures while *í*-XANES (X-ray absorption near edge structure) spectroscopy determinations revealed Cu to be present mainly as Cu(II) hydroxide and Cu(II) oxide. The reported results could be useful as a basic knowledge for planning new technologies for the on site physicochemical stabilization of heavy metals in heavily polluted soils.
- R. Terzano, M. Spagnuolo, L. Medici, F. Tateo, B. Vekemans, K. Janssens, P. Ruggiero, "Spectroscopic investigation on the chemical forms of Cu during the synthesis of zeolite X at low temperature", accepted in Applied Geochemistry, to appear in 2006.
  Abstract: The direct synthesis of zeolites in polluted soils has proved to be a promising process for the stabilisation of toxic metals inside these minerals. More detailed information about this process is still needed in order to better foresee the fate of heavy metals in treated soils. In this work zeolite X has been synthesized under alkaline conditions in an aqueous solution containing 2500 mg kg-1 of Cu, starting from sodium silicate and aluminium hydroxide at 60°C. Aluminium, Si, and Cu concentration in the aqueous phase, during zeolite synthesis, has been measured over a period of 160 hours. The solid products have been characterized over time by SEM-EDX, ESR, FT-IR, and synchrotron radiation X-ray diffraction (μ-XRD), X-ray fluorescence (μ-XRF) and X-ray microbeam Absorption Near Edge Structure (μ-XANES) and Extended X-ray Absorption Fine Structure (μ-EXAFS) spectroscopy. It appears that the marked reduction of Cu concentration in solution is not only due to a simple precipitation effect, but also to processes connected with the formation of zeolite X which could entrap, inside its porous structure, nano- or microocclusions of precipitated copper hydroxides and/or oxides. In addition, EXAFS

observations strengthen the hypothesis of the presence of different Cu phases even at a short-range molecular level and let suppose that some of these occlusions could be even bound to the zeolite framework. All the reported findings could be of particular interest since the discussed process could be technologically driven in order to reduce the availability of heavy metals in polluted soils.

5. Conferences and Meetings

2004

Annual meeting of the German Mineralogical Society - DMG, Karlsruhe- Dozentenvortrag

- From Heaven to Hell - Quantitative Nanopetrologie – Eur. J. Mineral., Bh., 16, 23, BRENKER, F.E. (2004)

Annual meeting of the German Mineralogical Society - DMG , Karlsruhe

- VINCZE, L., VEKEMANS, B., KERSTEN, M., NASDALA, L., BRENKER, F.E., VOLLMER, C., DRAKOPOULOS, M., RICKERS, K., FALKENBERG, G. & ADAMS, F. (2004) X-ray fluorescence microtomography and polycapillary based confocal imaging using synchrotron radiation - Eur. J. Mineral., Bh., 15, 151.

2005

ESRF-CNRS Workshop on "Synchrotron Radiation in Art and Archaeology", 9-11 February 2005, Grenoble, France

- *SR Techniques: new and future applications*, K. Janssens, opening lecture.

AIRMON05 - Fifth International Symposium on Modern Principles of Air Monitoring (including biomonitoring), Loen, Norway , June 12-16, 2005

- Speciation of Ni in the Monchegorsk aerosol, K. Janssens, plenary lecture

2005 Denver X-ray Conference (DXC2005), Colorado Springs, Colorado, USA (1-5 August 2005)

- *Towards, 3D Trace Element Microscopic XRF Analysis*; B. Vekemans, L. Vincze, K. Janssens. invited lecture.

Microscopy & Microanalysis, Waikiki Beach Hilton,Honolulu, August 2005

- Confocal X-ray Fluorescence Imaging and XRF Tomography for Three-Dimensional Trace Element Microanalysis, L. Vincze, invited lecture
- Analytical Instrumentation for Nano-Analysis, F. Adams, invited lecture

Chinese X-ray Analysis Meeting, JiuJiang, P.R. China, 24-28 October 2005

- The use of X-ray micro beams for characterization of geological and environmental materials at the microscopic level. K. Janssens, plenary lecture

1st European X-ray Analysis Society Workshop on Quantitative Analysis in X-ray Fluorescence Spectrometry, Ghent, Belgium, 13-14 October 2005

- Towards three-dimensional trace element microscopic XRF analysis", B. Vekemans, invited lecture

Annual meeting of the German Mineralogical Society - DMG, Aachen

- X-ray imaging of the deep Earth, F. Brenker, L. Vincze, B. Vekemans, K. Janssens, C. Vollmer & F. Kaminsky (2005)

ESRF-Users meeting, Februari 2005, Grenoble, France

- X-ray imaging of the deep Earth, F. Brenker, invited lecture